Mechanics & Industry **21**, 528 (2020)
© A. Maillard et al., published by EDP Sciences 2020
https://doi.org/10.1051/meca/2020055

Mechanics & Industry

Available online at:
www.mechanics-industry.org

REGULAR ARTICLE OPEN ACCESS

Hydroacoustic modelling applied in hydraulic components: a test rig based experiment

Arnaud Maillard[1,2,*], Éric Noppe[1], Benoît Eynard[1], and Xavier Carniel[2]

[1] Université de Technologie de Compiègne, Laboratoire Roberval FRE CNRS 2012, CS 60319, 60203 Compiègne Cedex, France
[2] Centre technique des industries mécaniques (Cetim), 52 Avenue Félix-Louat, CS 80067, 60304 Senlis Cedex, France

Received: 12 February 2019 / Accepted: 16 June 2020

Abstract. The exponential increase of computational power has allowed the development of numerical simulation methods. Numerical simulation is widely used in the industries at all stages of the product development process: the design support, comparison between several solutions, final validation. Virtual prototyping and optimization methods enable to meet requirements from the first physical prototype. Hydraulic power transmission, which can be considered as a mature technology providing an unrivalled specific power, is widespread for Off-Road and On-Road vehicles. Nevertheless, this kind of technology has two identified weaknesses which are energetic efficiency and noise generated during the operation. In such a context, the proposed research project focuses on the modelling, the analysis and the simulation for a component set constituting a hydraulic transmission taking into account the flow and pressure ripples. Thus, this work deals with the modelling of fluid borne noise applied to a hydrostatic transmission. From the state-of-the-art on hydroacoustic spread laws, the paper introduces an original method for the modelling of the transition from frequency to temporal domain allowing an analysis of the unsteady behaviour of hydraulic systems. Then, this method is applied to characterize the hydroacoustic behaviour of a rigid pipe using a simulation software. Finally, the used experimental means are presented, as well as a correlation between real measurement and computational analysis applied for a rigid pipe.

Keywords: Numerical engineering / fluid borne noise / hydroacoustic analysis / hydraulic power

1 Introduction

Hydraulic systems are widespread for off-road and on-road vehicles due to the mature technology reputation of hydraulic transmission providing an unrivalled specific power. Nevertheless, this kind of technology has two identified weaknesses which are energetic efficiency and noise generated during the operation. The components responsible for this noise called 'active components' are hydraulic pumps and motors due to the flow fluctuation at their outputs which is the result of the kinematic variation and the oil compressibility (Fig. 1).

Each component connected to pump and/or motor has a specific impedance Z (Eq. (1)) which reacts to the flow fluctuation

$$Z = \frac{p}{Q}. \quad (1)$$

A component assembly to form a whole hydraulic system or circuit (pumps/motors, pipes, hoses, valves, actuators, etc.) may, if it is poorly designed, spread and even amplify this pressure ripples. Finally, this fluid borne noise generates vibration at the interfaces and so is the cause of a part of noise emitted by the whole hydraulic system. Noise is spread by the fluid, the structures and the air according to a hierarchy of components presented in Figure 2.

In order to support in a suitable design of a hydraulic system, it is necessary to provide a way to predict hydroacoustic phenomena using modelling, analysis and simulation software. This involves knowing the hydroacoustic characteristics of each component integrated in the hydraulic system which can be obtained either by measurements on test rig and/or by mathematical models.

The paper will review the wave propagation theory in a rigid pipe and then describe the principle of a test rig based on this wave propagation theory to measure the hydroacoustic characteristics for passive hydraulic components. Some typical results will be presented applied in a rigid pipe. Then, a modelling method will be used and

* e-mail: arnaud.maillard@utc.fr

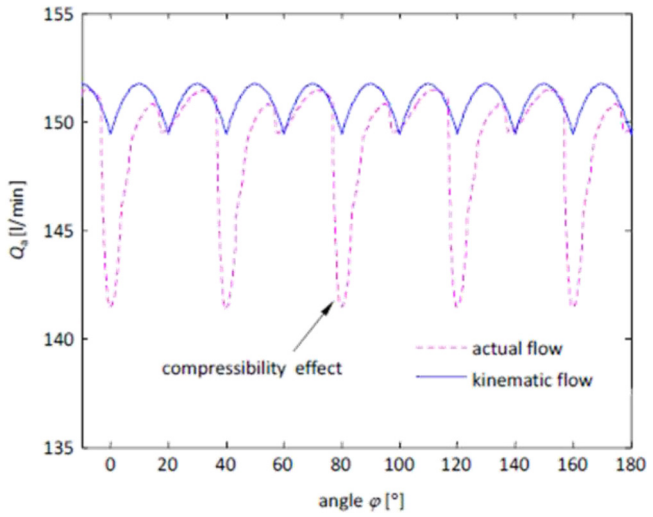

Fig. 1. Flow ripple characteristics for piston pumps.

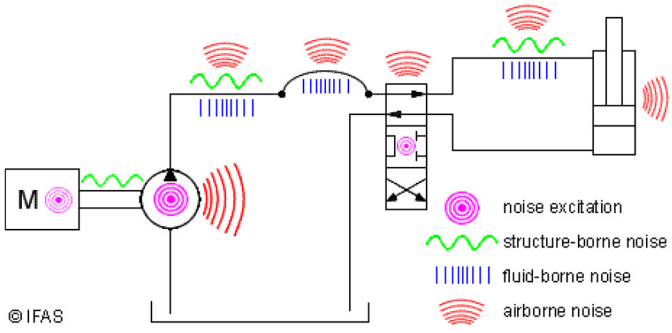

Fig. 2. Noise sources in a hydraulic circuit.

discussed to create a numerical model of a rigid pipe. Thus, the paper will end by a comparison between measurements and simulation results in order to assess the prediction of this numerical model.

2 Hydroacoustic characteristics for passive hydraulic components

This subsection is an overview of hydroacoustic characteristics for different hydraulic components described in frequency domain. These characteristics have to be specific for each component, i.e. which is independent of the remaining of the hydraulic circuit connected to it. As mentioned in the introductory section, hydroacoustic characteristics for each hydraulic component use the notion of impedance Z (Eq. (1)) or the notion of admittance Y which is the reciprocal of Z. Thus, the hydroacoustic characteristics of a passive hydraulic component are represented as a square matrix relating the pressure and flow ripples whose dimension is equal to the number of its ports. Each term of this matrix is a vector of complex numbers according to a frequency range. Characterizing a component means to define each matrix term depending on a mathematical modelling or by characterization on

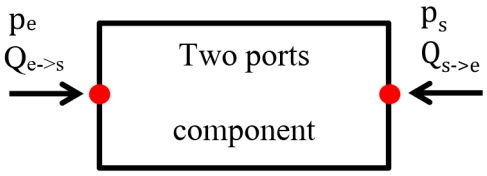

Fig. 3. Diagram of a two ports component.

a test rig. The example of a two ports component is proposed in Figure 3.

The impedance matrix relating the pressures as outputs and flows as inputs (Eq. (2)) and the admittance matrix (Eq. 3) which is the reciprocal are described below.

$$\begin{bmatrix} p_e \\ p_s \end{bmatrix} = \begin{bmatrix} Z_{11} & Z_{12} \\ Z_{21} & Z_{22} \end{bmatrix} \begin{bmatrix} Q_{e\to s} \\ Q_{s\to e} \end{bmatrix} \tag{2}$$

$$\begin{bmatrix} Q_{e\to s} \\ Q_{s\to e} \end{bmatrix} = \begin{bmatrix} Y_{11} & Y_{12} \\ Y_{21} & Y_{22} \end{bmatrix} \begin{bmatrix} p_e \\ p_s \end{bmatrix}. \tag{3}$$

Flow ripples ($Q_{s\to e}$ and $Q_{e\to s}$) are always considered as positive if they are entering in the rigid pipe portion studied.

In the case of a one port component, impedance or admittance matrix has just the first term Z_{11} or Y_{11}. Moreover, for certain components (valves, orifices, etc.), these different terms vary according to their operating points (mean pressure, mean flow rate, etc.). A state-of-the-art on the hydroacoustic characteristics for different hydraulic components and on different experimental means is discussed in the papers [1,2].

3 Mathematical modelling of wave propagation in a rigid pipe in the frequency domain

The wave propagation laws for a rigid pipe are well known and are the basis of the experimental means for modelling the active and passive hydraulic components as proposed in the papers [1,2].

For the considered research project, the used mathematical model for wave propagation in a rigid pipe is described in ISO standard 15086-1 [3]. The admittance matrix terms are defined by equations which are only dependent on geometric features of the rigid pipe (internal diameter d and length L) and oil features (density ρ, kinematic viscosity ν and speed of sound in oil c). The main advantage is to be dispensed with measurements on a test rig. Below is expressed the admittance matrix for a rigid pipe (Eq. (4)):

$$Y = \begin{bmatrix} A & B \\ B & A \end{bmatrix}. \tag{4}$$

As a rigid pipe is symmetrical, the admittance matrix Y is also symmetrical. This means that the wave propagation is independent of the mounting orientation of the rigid pipe. Both terms A and B of the admittance matrix are

expressed in equations from (5) to (8).

$$A = \frac{\pi d^2}{4\rho c^2}\frac{\omega L}{a - jb}\coth[j(a - jb)] \tag{5}$$

$$B = \frac{\pi d^2}{4\rho c^2}\frac{\omega L}{a - jb}\frac{j}{\sin(a - jb)} \tag{6}$$

where

$$a = \frac{L}{c}\left(\omega + \sqrt{\frac{2\omega\nu}{d^2}}\right) \tag{7}$$

$$b = \frac{L}{c}\left(\frac{4\nu}{d^2} + \sqrt{\frac{2\omega\nu}{d^2}}\right). \tag{8}$$

4 Experimental characterization for passive hydraulic components

Different passive hydraulic components have been characterized in the papers [4–7] with different test rigs. The hydroacoustic characteristics of the tested components are obtained from dynamic pressures measurement in a rigid pipe connected at the inlet port of the component. However, in these papers, there are not in general dynamic pressures measurements at the outlet port because the test rigs are designed in a way to be able to neglect the downstream impedance of the tested component or by taking into account this impedance in the calculation.

In order to not include this kind of uncertainties in the characterization, dynamic pressure measurements are performed at the inlet and outlet of the tested component. The principle of the test rig, presented in the paper in order to characterize passive hydraulic components, is based on the ISO standard 15086-3 [8]. The test rig has to be able to generate pressure ripples in the desired frequency range for different working conditions in mean pressure and mean flow rate. This implies to provide a working condition (a mean pressure and a mean flow rate) and then to superimpose on it flow and pressure ripples. Based on this generated pressure ripples, the admittance matrix terms are obtained from the tested component by measuring it with dynamic pressure sensors. Hydroacoustic characterization is processed by measuring the wave propagation characteristics of pressure ripples in a reference rigid pipe. As a matter of fact, the mathematical model for wave propagation in a rigid pipe is well known according to its physical characteristics in order to determine the pressure and flow ripples at each port of the tested component. If the speed of sound in oil is not known according to the pressure and the temperature, it has to be measured by using three dynamic pressure sensors. Else, only two dynamic pressure sensors are sufficient to compute the flow ripples. In this case, the temperature and the mean pressure have to be measured. The main advantage for using only two sensors is to limit the distance between the pulse generator and the farthest pressure sensor to have the best signal-to-noise ratio possible.

4.1 Distance between dynamic pressure sensors

The distance between the two dynamic pressure sensors of the reference rigid pipe used on the test rig depends on the frequency range desired according to the ISO standard 15086-2 [9]. The distance is chosen according to the maximum frequency by the equation (9):

$$L_{\text{sensors}} \leq \frac{0.95 * c}{2 * f_{\max}}. \tag{9}$$

Then, the minimum frequency resulting of this choice of distance has to be checked by the equation (10):

$$f_{\min} = f_{\max}\frac{d\theta * 10}{180}. \tag{10}$$

If the minimum frequency is higher than the desired value, the use of three sensors is necessary.

For the test rig, the distance between the two dynamic pressure sensors is 400 mm taking a value of 1300 m/s for the speed of sound in oil and for a maximum desired frequency of 1500 Hz. The minimum frequency for the measurements is therefore about 41 Hz taking into account the phase precision of the Fourier analyser $d\theta$ of 0.5°.

4.2 Rig construction

Figure 4 presents a diagram of the test rig for the hydroacoustic characterization of passive hydraulic components. The hydraulic power supply is done by a pump regulated in pressure (number 1 on Fig. 4) in order to maintain a constant pressure. The maximum pressure of the hydraulic power supply is 280 bar. This pump is connected to the test rig through a long distance of hoses and rigid pipe in order to attenuate the pressure ripples generated by the pump. In order to have an inlet pressure of the test bench the most constant, stable, an accumulator (number 3 on Fig. 4) is inserted at the beginning of the hydraulic circuit of the test bench. In order to characterize the component tested for different working conditions, two servo-valves are used. One servo-valve (number 5 on Fig. 4) is used to maintain the mean pressure desired in the test rig by a pressure control loop using a "classical" pressure sensor (P on Fig. 4). The second (number 4 on Fig. 4) is a high-frequency response servo-valve which generates pressure ripples in the frequency range from 40 Hz to 1500 Hz by sending it a white noise signal at this frequency range. The component tested is connected to the test rig through two identical reference rigid pipes (number 6 on Fig. 4) having two dynamic pressure sensors (P_1, P_2 and P_3, P_4) whose one of which is placed as close as possible to the component port. These reference rigid pipes must have approximately the same diameter of the component tested in order to avoid any flow disturbance which could be an important source of errors for the characterization. The adjustment of the mean flow rate is accomplished by adjusting the opening

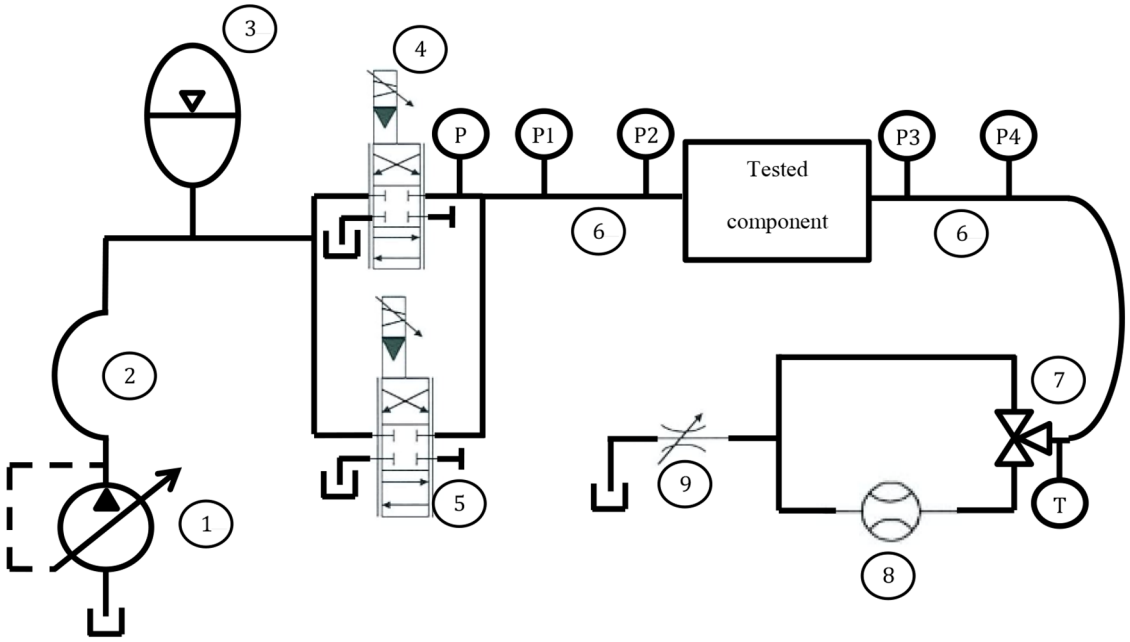

Fig. 4. Diagram of the test rig.

area of the flow restrictor (number 9 on Fig. 4) from the value measured by a flowmeter (number 8 on Fig. 4). When the mean flow rate is adjusted, the flowmeter can be shunted by a 3-way valve in the case where it is noted an impact of this sensor on the pressure ripples in the test rig.

4.3 Test procedure

The mean pressure in the test rig is set and the mean flow rate is adjusted by manipulating the flow restrictor. Then, the white noise signal is applied to the high-frequency response servo-valve and adjusted by an equalizer in order to have a good signal-to-noise ratio in all the frequency range. After checking to be on a stabilize condition for the mean pressure, the pressure ripples and the oil temperature, these different physical quantities are acquired in the temporal domain. In the case of a symmetrical component, only one measurement is needed but if the component is not symmetrical, the measurements have to be also achieved by returning the component on the test rig in order to acquire new data where pressure ripples are applied at the other port of the component.

4.4 Measurements analysis

Once acquired, a Fourier analysis is performed for the four dynamic pressure sensors in order to compute their spectral module. Their phases are computed by a frequency response function (FRF) analysis taking the dynamic pressure sensor P_2 (Fig. 4) as reference. Thus, all of the pressure ripples captured are determined in the frequency domain. Moreover, the coherence for each sensor is computed in order to check the validity of this pressure ripples data. The coherence values have to be greater than

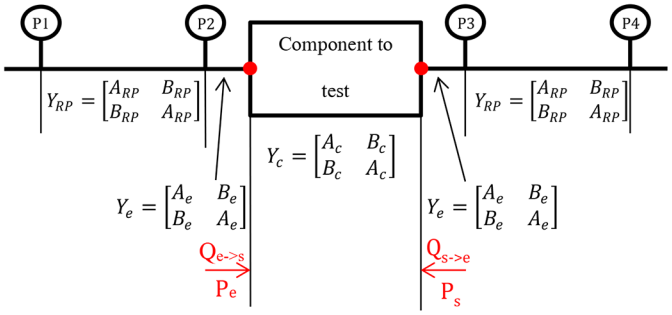

Fig. 5. Hydroacoustic parameters for a two-port component.

0.96 to be taken into account in the calculation of the admittance matrix terms. As the admittance matrix of a symmetrical component is also symmetrical, the algorithms to determine the admittance matrix terms are simpler than the algorithms explained in the ISO standard 15086-3 [8] which is valid for all kinds of passive hydraulic components.

Figure 5 shows the parameters for the hydroacoustic characterization of a symmetrical two-port component.

From the mathematical model for wave propagation in a rigid pipe and the oil characteristics, the admittance matrix terms between the two sensor pairs (P1, P2) and (P3, P4) are computed. This mathematical model gives the both matrix equations (Eqs. (11) and (12))

$$\begin{bmatrix} Q_{1\to 2} \\ Q_{2\to 1} \end{bmatrix} = \begin{bmatrix} A_{RP} & B_{RP} \\ B_{RP} & A_{RP} \end{bmatrix} \begin{bmatrix} p_1 \\ p_2 \end{bmatrix} \tag{11}$$

$$\begin{bmatrix} Q_{3\to 4} \\ Q_{4\to 3} \end{bmatrix} = \begin{bmatrix} A_{RP} & B_{RP} \\ B_{RP} & A_{RP} \end{bmatrix} \begin{bmatrix} p_3 \\ p_4 \end{bmatrix}. \tag{12}$$

From this both matrix equations, the flow ripples at the P2 and the P3 dynamic pressure sensors in the direction of the tested component are expressed respectively in equations (13) and (14).

$$Q_{2\to e} = -Q_{2\to 1} = -(B_{RP}p_1 + A_{RP}p_2) \tag{13}$$

$$Q_{3\to s} = -Q_{3\to 4} = -(A_{RP}p_3 + B_{RP}p_4). \tag{14}$$

Then, the mathematical model describes on matrix equations (15) and (16). Equations (15) and (16) respectively present the wave propagation in a rigid pipe applied in the rigid pipe portions between the dynamic pressure sensor P2 and the tested component and between the dynamic pressure sensor P3 and the tested component.

$$\begin{bmatrix} Q_{2\to e} \\ Q_{e\to 2} \end{bmatrix} = \begin{bmatrix} A_e & B_e \\ B_e & A_e \end{bmatrix} \begin{bmatrix} p_2 \\ p_e \end{bmatrix} \tag{15}$$

$$\begin{bmatrix} Q_{3\to s} \\ Q_{s\to 3} \end{bmatrix} = \begin{bmatrix} A_e & B_e \\ B_e & A_e \end{bmatrix} \begin{bmatrix} p_3 \\ p_s \end{bmatrix}. \tag{16}$$

By substituting $Q_{2\to e}$ of the equation (13) in the matrix equation (15) and $Q_{3\to s}$ of the equation (14) in the matrix equation (16), the pressure ripples Pe and Ps are obtained (Eqs. (17) and (18)).

$$p_e = -\left[\frac{B_{RP}\,p_1 + (A_{RP} + A_e)p_2}{B_e}\right] \tag{17}$$

$$p_s = -\left[\frac{(A_{RP} + A_e)p_3 + B_{RP}\,p_4}{B_e}\right]. \tag{18}$$

Thus, from this pressure ripples p_e and p_s and the matrix equations (15) and (16), the flow ripples at both ports $Q_{e\to s}$ and $Q_{s\to e}$ can be computed (Eqs. (19) and (20))

$$Q_{e\to s} = -Q_{e\to 2} = \left[\frac{A_e B_{RP}\,p_1 + \left(A_e^2 - B_e^2 + A_e A_{RP}\right)p_2}{B_e}\right] \tag{19}$$

$$Q_{s\to e} = -Q_{s\to 3} = \left[\frac{\left(A_e^2 - B_e^2 + A_e A_{RP}\right)p_3 + A_e B_{RP}\,p_4}{B_e}\right]. \tag{20}$$

Now that the pressure and flow ripples are known at both ports of the tested component, the admittance matrix terms Ac and Bc can be calculated according to the matrix equation (21)

$$\begin{bmatrix} Q_{e\to s} \\ Q_{s\to e} \end{bmatrix} = \begin{bmatrix} A_c & B_c \\ B_c & A_c \end{bmatrix} \begin{bmatrix} p_e \\ p_s \end{bmatrix}. \tag{21}$$

Table 1. Oil characteristics at a mean pressure of 35 bar and a temperature of 45 °C.

Oil characteristics	Value
Kinematic viscosity, ν	36.93 cSt
Speed of sound, c	1335 m s^{-1}
Density, ρ	866 kg m^{-1}

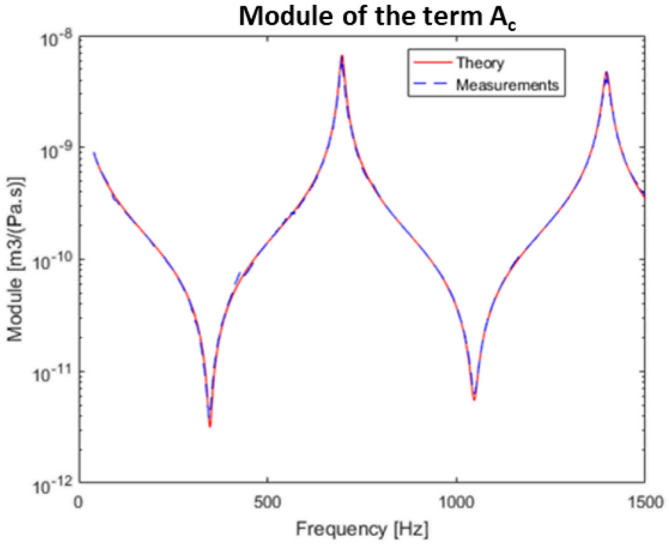

Fig. 6. Module comparison between theory and measurements for the term A_c.

Therefore, A_c and B_c are expressed respectively in the equations (22) and (23) below:

$$A_c = \frac{Q_{s\to e}\,p_s - Q_{e\to s}\,p_e}{p_s^2 - p_e^2} \tag{22}$$

$$B_c = \frac{Q_{e\to s} - A_c\,p_e}{p_s}. \tag{23}$$

4.5 Results applied in a rigid pipe

In this paper is presented a hydroacoustic characterization applied in a rigid pipe with a length of 950 mm and an internal diameter of 16 mm. The measurement has been performed at a mean pressure of 35 bar, and an oil temperature of 45 °C. At this working condition, the oil characteristics are expressed in Table 1.

Below the comparison for the term A_c between the theory and the measurements in Figure 6 for the module and in Figure 7 for the phase.

Below the comparison for the term B_c between the theory and the measurements on Figure 8 for the module and in Figure 9 for the phase.

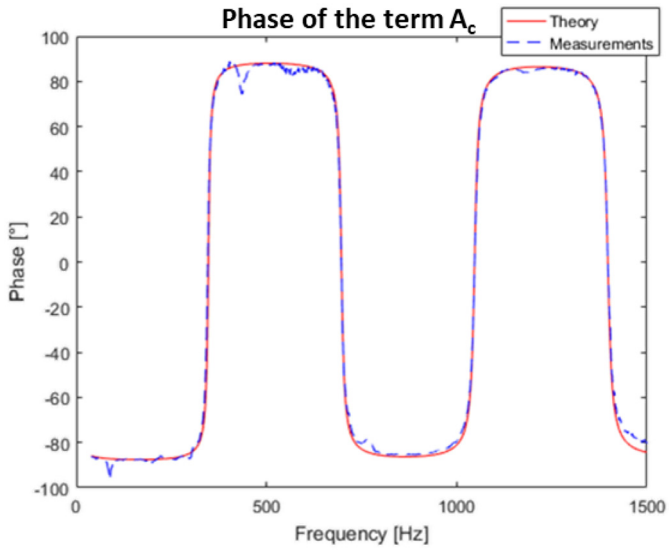

Fig. 7. Phase comparison between theory and measurements for the term A_c.

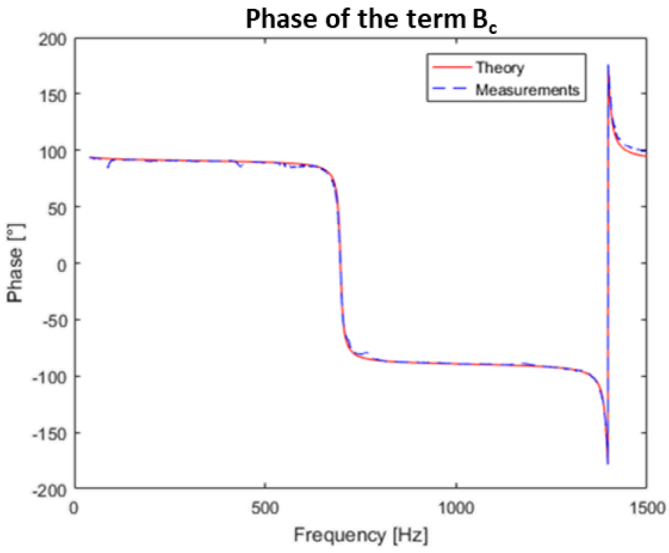

Fig. 9. Phase comparison between theory and measurements for the term B_c.

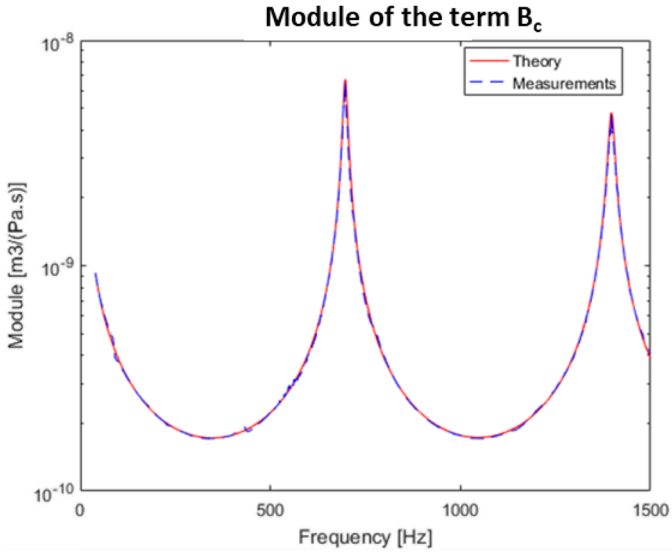

Fig. 8. Module comparison between theory and measurements for the term B_c.

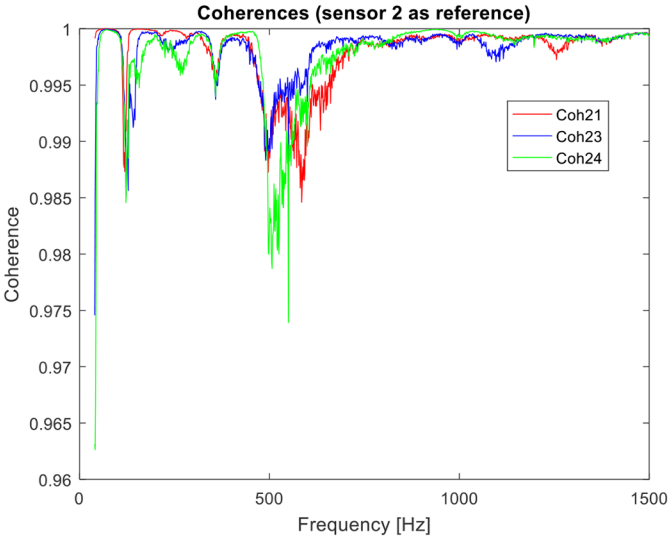

Fig. 10. Coherences of dynamic pressure sensors according to the sensor P_2.

The main interest to characterize a component, whose a mathematical model is well known, is to check if there is not any flow disturbance which could disrupt the pressure ripple measurements but also to validate the measurement analysis method. The results in modules and phases for both terms fit with a good accuracy the theory of the wave propagation in a rigid pipe, which validate these two points to check.

Figure 10 shows the coherence of each dynamic pressure sensors taking the sensor P_2 as reference. The coherence for each sensor is very good, this confirms that the rig construction is well suitable for the hydroacoustic characterization.

5 Rigid pipe numerical model taking into account fluid born noise

In order to be able to predict the pressure and flow ripples in a transient state, a huge effort to model/simulate hydraulic components or systems taking into account fluid born noise has been done in the papers [10–14] where a synthesis of the different existing models is presented in papers [1,15]. In general, these existing models require to make approximations of the wave propagation laws expressed in the frequency domain in order to implement them in temporal models.

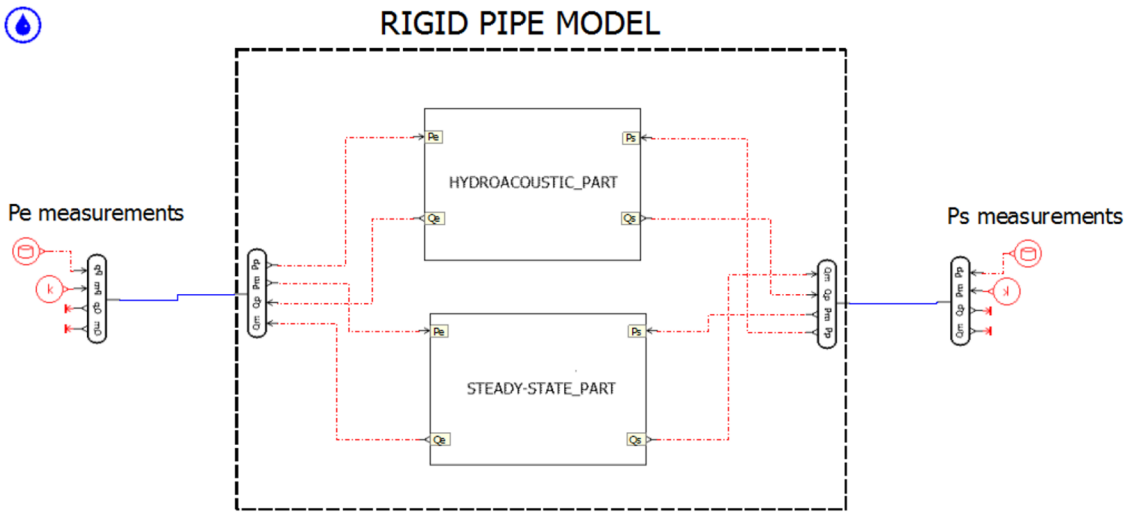

Fig. 11. Rigid pipe model in AMESim©.

5.1 Principle

A rigid pipe model has been created in AMESim© taking into account fluid born noise in a temporal domain modelling software. As the hydroacoustic characteristics are described in the frequency domain and do not take into account the steady-state of the pressure and flow ripples, two major issues have been encountered which are:

– The transition from the frequency to the temporal domain
– The modelling taking into account the steady-state and the dynamic pressure and flow rate.

As a matter of fact, the AMESim© software is not able to process frequency data during a simulation, that's why this data has to be transformed into the temporal domain to parameterize the hydroacoustic part of the rigid pipe model. This transition is explained in the following chapter. The steady-state is performed using the hydraulic component of a rigid pipe available in the hydraulic library in AMESim©. This existing component will only be connected with the steady-state part of other components in order to have the steady-state characteristics for pressure drop, flow rate etc.

Figure 11 shows the rigid pipe model which is constituted of the two main parts (hydroacoustic and steady-state part).

5.2 Transition from the frequency to temporal domain

The main purpose is to describe and characterize hydraulic components and its assembly in temporal domain using a modelling and simulation software. The different mathematical models in this field being described in frequency domain, it is necessary to translate impedance or admittance matrix terms from the frequency domain into the temporal domain. The transition method used in this paper is the "Vector fitting" according to papers [16–18]. This method defines a sum of rational approximation of first order to fit a vector in frequency domain as shown below in equation (24):

$$f(s) = \sum_{m=1}^{N} \frac{r_m}{s - a_m} + d_{vf} + s * e \tag{24}$$

where $f(s)$ is a vector in frequency domain, r_m and a_m are respectively the residue and poles for the mth rational function and N is the rational function number called "order of approximation". In our case, the equation (24) has been simplified by neglecting the coefficients d_{vf} and e by setting them to zero. This method is implemented in a Matlab© function called "rationalfit". The outputs of this function are the values of the residue r_m and the pole a_m of each first order rational function. To fit anti-resonance of the frequency response $f(s)$, this function can give complex poles and residues. When it is the case, this function always gives a couple of first order rational function which one has its residue and pole as the conjugate of the other. In order to avoid all first order rational function with complex numbers, each pair of functions with complex numbers is transformed into a second order rational function.

6 Comparison between the measurements and the simulation results for fluid born noise in a rigid pipe

The admittance matrix terms are computed according to the mathematical model for wave propagation in a rigid pipe and transformed into the temporal domain thanks to the rational approximation method called "Vector fitting". The order of approximation was set to 18. Each rational function of the admittance matrix terms obtained by the transition from the frequency domain to temporal domain is inserted in the AMESim© model of a rigid pipe. The inputs of the AMESim© model are the pressure at its ports. In this comparison, the pressure measurements in temporal domain obtained on a test rig were inserted (see Fig. 11)

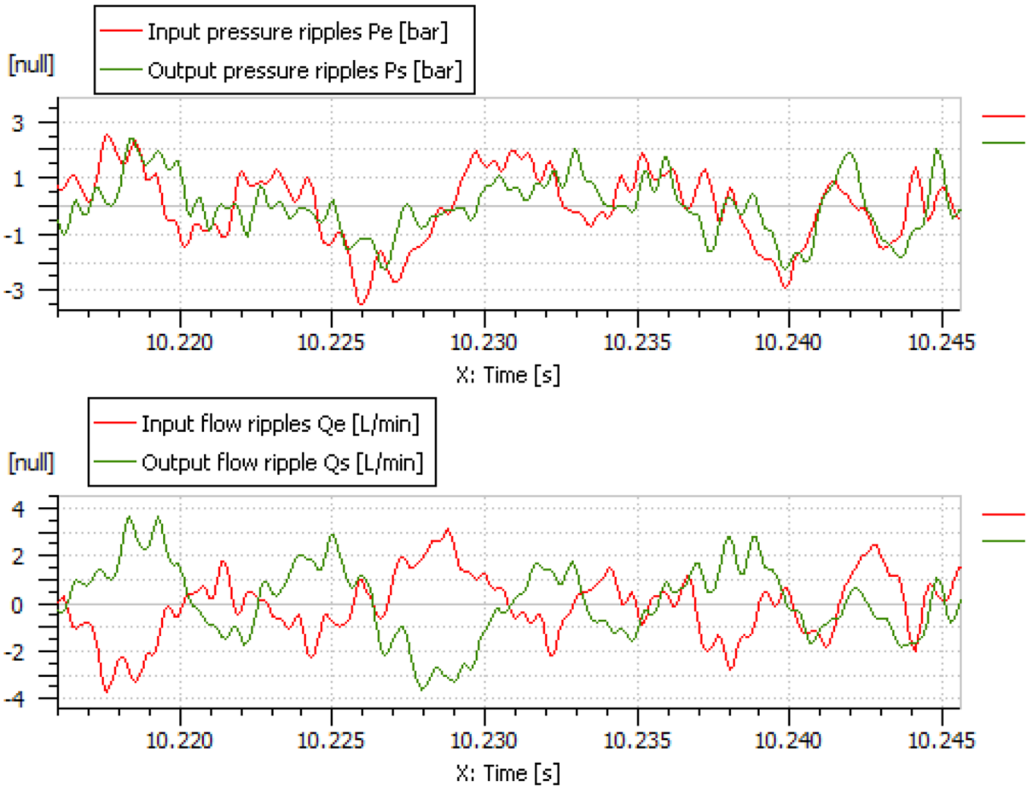

Fig. 12. Pressure and flow ripples at both component ports in AMESim© model.

and, therefore, the flow ripples were computed according to it. In Figure 12 are shown the inlet and outlet pressure and flow ripples obtained by the simulation.

The simulation results in temporal domain for the flow ripples at both ports in the AMESim© model are then processed in Matlab© in order to perform a spectral analysis of these flow ripples. Then the modules and phases obtained by measurement and by simulation are compared.

Below is presented the results for the module of the entering flow in the rigid pipe on Figure 13.

The simulation results fit the measurements with an excellent precision in all the frequency range. Now, it remains to check the phase which is very important to take into account interaction with other components connected to its ports. So, in Figure 14 shows the phase comparison between the measurements and the simulation results.

The phase comparison matches with a good precision in general except for some frequencies. The differences at these frequencies (around 585 Hz, at 1323 Hz and 1329 Hz) come from the FRF (Frequency Response Function) processed which keeps the phase between [−180°, 180°]. So, this artifact would not have an impact on the results at these frequencies. Indeed, a pure sinusoidal signal is identical for a phase of 180° or −180°.

The same comparison has been done for the output flow ripples $Q_{s\to e}$. On Figure 15 is compared the module of $Q_{s\to e}$, as for the input flow ripples $Q_{e\to s}$, the module obtained by the simulation has a good level of fidelity.

The phases of $Q_{s\to e}$ shown in Figure 16 obtained by measurements and by simulation are identical.

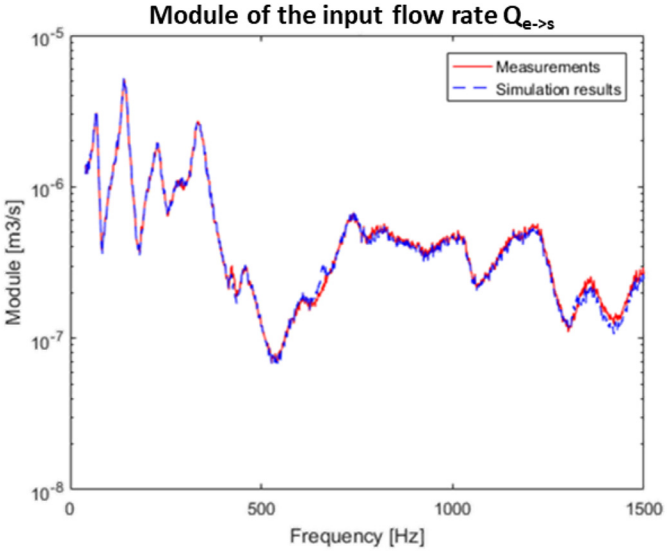

Fig. 13. Module comparison for the input flow ripples $Q_{e\to s}$.

These different comparisons allow the validation of the "modelling method" which consists to split up the dynamic modelling with the steady-state modelling for a component. Moreover, this can also validate that the transition from the frequency to the temporal domain is suitable to model the hydroacoustic behaviour of a passive hydraulic component.

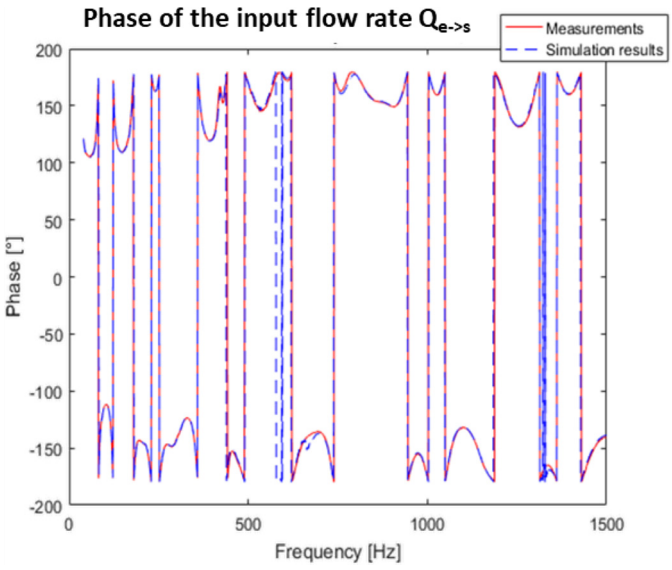

Fig. 14. Phase comparison for the input flow ripples $Q_{e\to s}$.

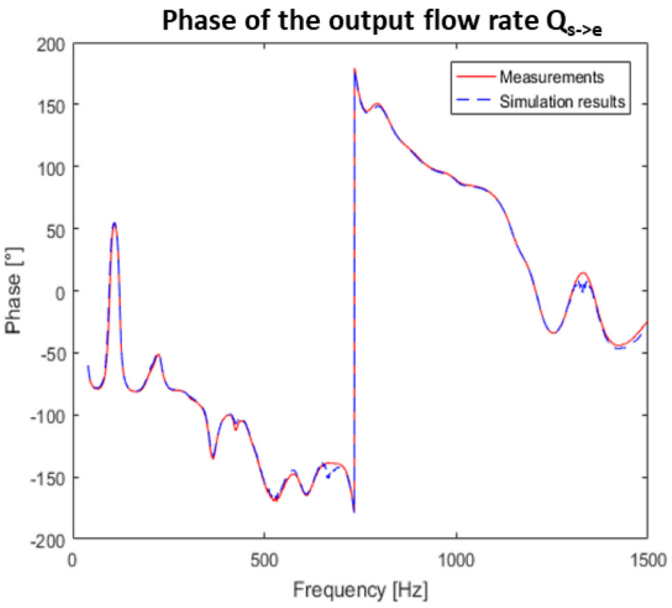

Fig. 16. Phase comparison for the Output flow ripples $Q_{s\to e}$.

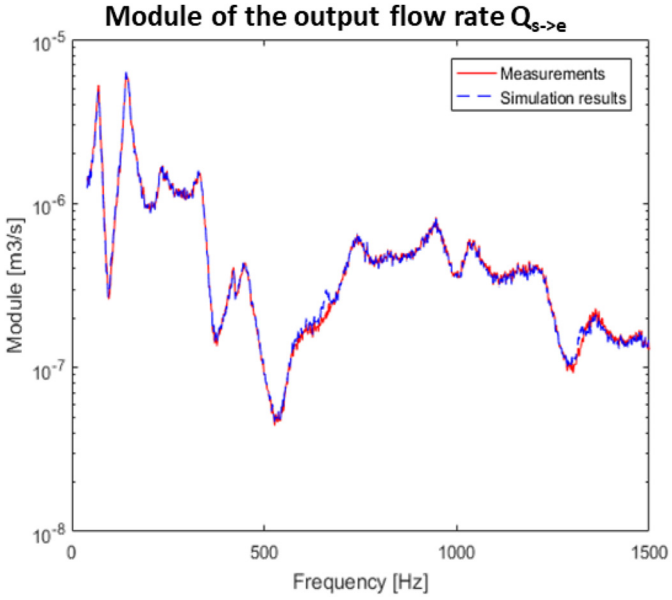

Fig. 15. Module comparison for the output flow ripples $Q_{s\to e}$.

7 Outlook

The test rig explained in this paper will be used to characterize a 90° elbow but also to characterize the interaction between two 90° elbows. As a matter of fact, even if the admittance matrix terms are known for an elbow, the connection of two elbows can't be modelled by applying twice this admittance matrix. Indeed, the admittance matrix terms are known for an inlet flow rate in laminar regime, however, in the case where there are two elbows connected together, the inlet flow rate of the second elbow is turbulent, which change the admittance matrix terms. This test rig has been studied to characterize this interaction according to mean pressure and mean flow rate. So, a 90° elbow will be characterized, and then a characterization of two elbows connected together will be processed. Furthermore, the hydroacoustic modelling method described in this paper will be applied for others hydraulic components such as pumps/motors, hoses, accumulators.

8 Conclusion

The results obtained with the test rig for the rigid pipe characterization, whose the mathematical model for wave propagation is well known, have been found as sufficiently accurate to validate the test rig. This allows forecasting the characterization of other passive hydraulic components and particularly for the characterization of the interaction between components.

The comparison of the numerical model of a rigid pipe according to measurements done with the test rig has shown a very good correlation which validates especially the transition from the frequency to the temporal domain, necessary to simulate the hydroacoustic behaviour in the temporal simulation software AMESim©.

Nomenclature

A_c, B_c	Admittance matrix terms of the tested component ($m^3\,Pa^{-1}\,s^{-1}$)
A_e, B_e	Admittance matrix terms of the rigid pipe portion between sensor and the tested component ($m^3\,Pa^{-1}\,s^{-1}$)
A_{RP}, B_{RP}	Admittance matrix terms of a rigid pipe ($m^3\,Pa^{-1}\,s^{-1}$)
a_m	Pole for the mth first order rational approximation
A_{RP}, B_{RP}	Admittance matrix terms of the reference rigid pipe ($m^3\,Pa^{-1}\,s^{-1}$)
c	Speed of sound in oil ($m\,s^{-1}$)

d	Diameter (m)
d_{vf} and e	Coefficients for the vector fitting method
$f(s)$	Frequency response of a term
$f_{\max}$	Maximum frequency for the measurement (Hz)
$f_{\min}$	Minimum frequency for the measurement (Hz)
j	Complex number
L	Length (m)
L_{sensors}	Sensor spacing (m)
P_i	Pressure sensor at the position i (Pa)
p_i	Pressure ripples at the position i (Pa)
$Q_{i->j}$	Flow ripple at the position i directed to the position j ($\mathrm{m^3\,s^{-1}}$)
r_m	Residue for the mth first order rational approximation
s	Laplace variable ($s = j\omega$) ($\mathrm{rad\,s^{-1}}$)
Y	Admittance matrix ($\mathrm{m^3\,Pa^{-1}\,s^{-1}}$)
Y_{ij}	Admittance matrix term at the row i and column j ($\mathrm{m^3\,Pa^{-1}\,s^{-1}}$)
Z	Impedance matrix ($\mathrm{Pa\,s\,m^{-3}}$)
Z_{ij}	Impedance matrix term at the row i and column j ($\mathrm{Pa\,s\,m^{-3}}$)
$d\theta$	Phase precision of the Fourier analyser°
ν	Oil kinematic viscosity ($\mathrm{m^2\,s^{-1}}$)
ρ	Oil density ($\mathrm{kg\,m^{-3}}$)
ω	Angular velocity ($\mathrm{rad\,s^{-1}}$)

References

[1] A. Maillard, E. Noppe, B. Eynard, X. Carniel, Ingénierie système et modélisation hydroacoustique appliquées aux composants hydrauliques de puissance, in 22ème Congrès Français de Mécanique, 24–28 aoÛt2015, Lyon, France (FR), AFM, 2015

[2] A. Maillard, E. Noppe, B. Eynard, X. Carniel, Systems engineering and hydroacoustic modelling applied in simulation of hydraulic components, in *Proceedings of the International Joint Conference on Mechanics, Design Engineering & Advanced Manufacturing (JCM 2016), Catania, Italy*, 2016, 687–696

[3] ISO 15086-1, Hydraulic Fluid Power: Determination of the Fluid-Borne Noise Characteristics of Components and Systems-Part 1: Introduction, 2001

[4] D.N. Johnston, K.A. Edge, M. Brunelli, Impedance and stability characteristics of a relief valve, Proc. Inst. Mech. Eng. I **216**, 371–382 (2002)

[5] K.K. Lau, K.A. Edge, D.N. Johnston, Impedance characteristics of hydraulic orifices, Proc. Inst. Mech. Eng. I **209**, 241–253 (1995)

[6] K.A. Edge, D.N. Johnston, The impedance characteristics of fluid power components: relief valves and accumulators, Proc. Inst. Mech. Eng. I **205**, 11–22 (1991)

[7] D.N. Johnston, K.A. Edge, The impedance characteristics of fluid power components: restrictor and flow control valves, Proc. Inst. Mech. Eng. I **205**, 3–10 (1991)

[8] ISO 15086-3, Hydraulic Fluid Power: Determination of the Fluid-Borne Noise Characteristics of Components and Systems-Part 3: Measurement of Hydraulic Impedance, 2008

[9] ISO 15086-2, Hydraulic Fluid Power: Determination of the Fluid-Borne Noise Characteristics of Components and Systems-Part 2: Measurement of the speed of sound in a Fluid in a Pipe, 2000

[10] S.E.M. Taylor, D.N. Johnston, D.K. Longmore, Modelling of transient flow in hydraulic pipelines, Proc. Inst. Mech. Eng. I **211**, 447–455 (1997)

[11] P. Wongputorn, D. Hullender, R. Woods, J. King, Application of MATLAB functions for time domain simulation of systems with lines with fluid transients, J. Fluids Eng. **127** (2005)

[12] S.V.H. Tummescheit, Implementation of a transmission line model for fast simulation of fluid flow dynamics, in *Proceedings 8th Modelica Conference, Dresden, Germany*, 2011, pp. 446–453

[13] N. Johnston, The Transmission Line Method for Modelling Laminar Flow of Liquid in Pipelines, Proc. Inst. Mech. Eng. I **226**, 586–589 (2012)

[14] D.N. Johnston, An enhanced transmission line method for modelling laminar flow of liquid in pipelines, Proc. Inst. Mech. Eng. I **228**, 193–206 (2014)

[15] M. Soumelidis, D.N. Johnston, K.A. Edge, D.G. Tilley, A comparative study of modelling techniques for laminar flow transients in hydraulic pipelines, in *Proceedings of the 6th JFPS International Symposium on Fluid Power, TSUKUBA, Japan*, 2005, 100–105

[16] B. Gustavsen, A. Semlyen, Rational approximation of frequency domain responses by vector fitting, IEEE Trans. Power Del. **14**, 1052–1061 (1999)

[17] B. Gustavsen, Improving the pole relocating properties of vector fitting, IEEE Trans. Power Del. **21**, 1587–1592 (2006)

[18] D. Deschrijver, M. Mrozowski, T. Dhaene, D. De Zutter, Macromodeling of multiport systems using a fast implementation of the vector fitting method, IEEE Microw. Wireless Comp. Lett. **18**, 383–385 (2008)

Cite this article as: A. Maillard, É. Noppe, B. Eynard, X. Carniel, Hydroacoustic modelling applied in hydraulic components: a test rig based experiment, Mechanics & Industry **21**, 528 (2020)